

Transport Properties and Electronic Phase Diagram of Single-Crystalline $\text{Ca}_{10}(\text{Pt}_3\text{As}_8)((\text{Fe}_{1-x}\text{Pt}_x)_2\text{As}_2)_5$

Z. J. Xiang, X. G. Luo, J. J. Ying, X. F. Wang, Y. J. Yan, A. F. Wang, P. Cheng, G. J. Ye, and X. H. Chen*
*Hefei National Laboratory for Physical Science at Microscale and Department of Physics,
 University of Science and Technology of China, Hefei,
 Anhui 230026, People's Republic of China*

Sizable single-crystalline samples of $\text{Ca}_{10}(\text{Pt}_3\text{As}_8)((\text{Fe}_{1-x}\text{Pt}_x)_2\text{As}_2)_5$ (the 10-3-8 phase) with $0 \leq x < 0.1$ have been grown and systematically characterized via X-Ray diffraction, magnetic, and transport measurements. The undoped sample is a heavily doped semiconductor with no sign of magnetic order down to 2 K. With increasing Pt content, the metallic behavior appears and superconductivity is realized for $x \geq 0.023$. T_c rises to its maximum of approximately 13.6 K at the doping level of $x \sim 0.06$, and then decreases for higher x values. The electronic phase diagram of the 10-3-8 phase was mapped out based on the transport measurements. The mass anisotropy parameter $\Gamma \sim 10$ obtained from resistive measurements in magnetic fields indicates a relatively large anisotropy in the iron-based superconductor family. This strong 2D character may lead to the absence of magnetic order. A linear T -dependence of susceptibility at high temperature is observed, indicating that spin fluctuations exist in the underdoped region as in most of the Fe-pnictide superconductors.

PACS numbers: 74.25.-q, 74.25.Ha, 74.25.F-, 74.25.Dw, 74.70.Dd

I. INTRODUCTION

In the discovered high-temperature superconductors, which include cuprates and iron-based superconductors, superconductivity is often found in proximity to a magnetically ordered state. The parent compounds of cuprates are antiferromagnetic insulators while for iron-based superconductors the parent compounds are antiferromagnetic "semimetals". By charge injection via chemical substitution, magnetic order is suppressed and superconductivity appears in both of these two families. It is widely accepted nowadays that there is an intimate association between magnetism and superconductivity in the high-temperature superconductors. Different from the cuprates, in which Mott physics is dominant and the magnetic order is a Heisenberg AFM order of localized spins, the magnetic order of the Fe-pnictides is spin-density wave (SDW) type and exhibits a significant itinerant character. Most of Fe-pnictide superconductors have SDW region next to or overlapping with the superconducting region in their electronic phase diagrams¹⁻⁵. Many theories suggest that the spin dynamics play a crucial role in the pairing mechanism for the superconductivity in the Fe-pnictide superconductors^{6,7}, and it is conjectured that AFM spin fluctuations mediate the s_{\pm} pairing and are responsible for the high T_c in Fe-pnictides⁸⁻¹⁰. However, there are several kinds of Fe-pnictide superconductors that have no report about the existence of long-range magnetic order, such as LiFeAs ¹¹ and so-called "perov-FeAs" materials. The latter is a group of layered materials in which FeAs layers were sep-

arated by perovskite-type layers. The chemical formula of perov-FeAs is either $(\text{Ae}_{n+1}\text{MnO}_{3n-1-y})(\text{Fe}_2\text{Pn}_2)$ or $(\text{Ae}_{n+2}\text{MnO}_{3n-y})(\text{Fe}_2\text{Pn}_2)$, with $\text{Ae} = \text{Ca}, \text{Sr}, \text{Ba}$ and $\text{M} = \text{Mg}, \text{Al}, \text{Sc}, \text{Ti}, \text{V}, \text{Cr}, \text{Co}$, etc.¹²⁻¹⁶, among which the highest T_c ever reported is ~ 47 K for $(\text{Ca}_4(\text{Mg}, \text{Ti})_3\text{O}_y)(\text{Fe}_2\text{As}_2)$ ¹⁷. All of these nonmagnetic Fe-pnictide materials are intrinsic superconductors that show superconductivity in the stoichiometric compound. Recently a new type of layered Fe-pnictide superconductor, $\text{Ca}_{10}(\text{Pt}_n\text{As}_8)((\text{Fe}_{1-x}\text{Pt}_x)_2\text{As}_2)_5$ (the 10- n -8 phase, $n = 3, 4$) was discovered¹⁸⁻²⁰. These materials have complex crystal structure with triclinic symmetry (space group $P-1$), in which Fe_2As_2 layers alternate with Pt_nAs_8 layers forming a $-\text{Ca}-(\text{Pt}_n\text{As}_8)-\text{Ca}-(\text{Fe}_2\text{As}_2)-$ stacking. We noticed that for the 10-3-8 phase the stoichiometric compound $\text{Ca}_{10}(\text{Pt}_3\text{As}_8)(\text{Fe}_2\text{As}_2)_5$ was non-superconducting and show no visible magnetic transitions, while electron doping through partial replacing Fe by Pt in the Fe_2As_2 layers induced superconductivity. These characters were special in the family of Fe-pnictide superconductors. In this paper, we report the results of a systematic study of the transport and magnetic properties of single-crystalline $\text{Ca}_{10}(\text{Pt}_3\text{As}_8)((\text{Fe}_{1-x}\text{Pt}_x)_2\text{As}_2)_5$ in different doping regions, and present a corresponding electronic phase diagram. All the data indicated that there is no magnetic order in this system. The undoped sample is a semiconductor instead of a SDW semimetal. Superconductivity emerges upon 5d-transition metal Pt substituting on the Fe site, as in the case of Pt-doped 122 type Fe-pnictide superconductors^{21,22}. T_c reaches its maximum ~ 13.6 K at the doping level $x \sim 0.06$, and further doping slowly suppresses T_c . The overdoped samples gradually exhibit a phase separation so that the SC region is not a perfect dome-shape one. We also mentioned that the AFM spin fluctuations still exist in this system

*Corresponding author; Electronic address: chenxh@ustc.edu.cn

as well as in other Fe-pnictide superconductors, and the reason for the absence of AFM order might be ascribed to the highly anisotropy in the 10-3-8 phase.

II. EXPERIMENTAL RESULTS

Single crystals of 10-3-8 sample were grown by self-flux method. Precursors CaAs and FeAs were prepared by reacting the mixture of the element in the evacuated quartz tubes at 923 K for 24 h, and at 973 K for 12 h, respectively. The starting material CaAs, FeAs and Pt were mixed by a ratio of 2:2:(0.6+x) ($x = 0, 0.1, 0.2, 0.3, 0.4$) in an Argon-filled glovebox, thoroughly ground and put into alumina crucibles. The crucibles were sealed in an evacuated quartz tube, and then heated to a temperature above 1273 K at a rate of 100 K/h. For the superconducting samples, the best reaction temperature is 1323 K. The tubes were kept at this temperature for 75 hours and then cooled to 1173 K at a rate of 4.5 K/h. Finally the quartz tube was cooled in the furnace after shutting off the power. For the undoped compound, we chose higher reaction temperature as 1423 K and the reaction time was prolonged to 100 h, while the starting ratio of CaAs, FeAs and Pt was fixed at 2:2:1.05. After cooling we obtained several dark gray granules with typical dimension $4 \times 4 \times 3 \text{ mm}^3$ together with a little amount of gray powder in the crucibles. The shining plate-like 10-3-8 crystals were cleaved from the internal of the granules. Single crystals were characterized by x-ray diffraction (XRD) using Cu K_α radiation. The actual chemical composition of the single crystals was determined by energy dispersive X-ray spectroscopy (EDS). The in-plane electrical transport was measured with PPMS (Quantum Design Inc.) using the ac four-probe method. The Hall effect was measured by the four-terminal ac technique. Magnetic susceptibility of superconducting state was measured using a Quantum Design SQUID magnetometer. Normal state susceptibility was measured by a vibrating sample magnetometer (VSM).

III. RESULTS AND DISCUSSIONS

The typical size of cleaved single crystal is about $2 \times 3 \times 0.1 \text{ mm}^3$, as shown in Figure 1(a). Figure 1(b) shows the single crystal XRD patterns. Only (00l) reflections are observed, indicating that the single crystals are in perfect (001) orientation. The full width of half maximum (FWHM) in the rocking curve of the (004) peak is 0.09-0.20 degree, which indicates the single crystals are of high quality. Determined by the results of EDS, the atomic ratios of single crystals that cleaved from different granules in the same batch are slightly different, but the chemical composition is approximately uniform within one granule. The EDS results of samples from different starting material ratios are shown in table 1. The Pt doping concentrations in the Fe_2As_2 layer

were calculated from the relative atom ratio of iron and platinum by assuming that there are no Pt vacancy or Fe substitution in the Pt_3As_8 layer, according to the structure analysis in previous studies¹⁸⁻²⁰. When doping concentration $x > 0.075$, it became rather difficult to get pure 10-3-8 phase. The XRD pattern of single crystals in overdoped region usually shows two sets of (00l) diffraction peaks, one corresponds to 10-3-8 phase and the other has larger (001) spacing (more than 10.3 \AA), which can be attributed to the existence of so-called "10-4-8" phase^{18,19} intergrowing with 10-3-8 phase. The sample No.12 in table 1 with $x = 0.0981$, which is discussed in this paper as overdoped sample, does not show the intergrowing phenomenon. We did not succeed in growing single phase sample with doping level $x > 0.1$.

Figure 1(d) shows the powder XRD pattern of underdoped 10-3-8 phase. The powder was obtained by grounding single crystal pieces, and the Miller indices were marked according to a triclinic(P-1) unit cell symmetry. The lattice parameters determined by powder diffraction were estimated to be $a = 8.7608 \text{ \AA}$, $b = 8.7551 \text{ \AA}$, $c = 10.6831 \text{ \AA}$; $\alpha = 94.6823^\circ$, $\beta = 104.2267^\circ$, $\gamma = 89.9874^\circ$. These values are generally in accordance with former results¹⁸. Figure 1(e) presents the evolution trend of the interlayer distance of two neighboring Fe-Fe square plane with Pt doping into FeAs layers. The interlayer distance ($d(001)$) increasing rapidly in the underdoped region, and the variation slows down as approaching optimal doping. As for $x > 0.05$, the value of $d(001)$ almost unchanged with Pt content.

Figure 2 shows the temperature dependence of in-plane resistivity of $\text{Ca}_{10}(\text{Pt}_3\text{As}_8)((\text{Fe}_{1-x}\text{Pt}_x)_2\text{As}_2)_5$ single crystals. The behavior of resistivity of the undoped sample $\text{Ca}_{10}(\text{Pt}_3\text{As}_8)(\text{Fe}_2\text{As}_2)_5$ is obviously different from those of the undoped compound of the other iron-based superconductors. The parent compound of 1111 and 122 Fe-based superconductors are so-called "semimetal" and an abnormal feature in resistivity is observed at the SDW transition/structural transition^{23,24}. In this case, the undoped sample is a heavily doped semiconductor, and the resistivity increases with cooling in the entire temperature range from 300 K to 2 K. Below about 100 K a sharp increase in $-d\rho/dT$ is observed, but no magnetic anomaly was seen down to 2 K. The value of resistivity at room temperature is of the same order of magnitude with polycrystalline LaFeAsO ²⁵, one order of magnitude larger than BaFe_2As_2 single crystal, and one and two order of magnitude smaller than the non-superconducting $(\text{Sr}_4\text{Sc}_2\text{O}_6)(\text{Fe}_2\text{As}_2)$ ²⁶ and the semiconducting phase of $\text{K}_x\text{Fe}_{2-y}\text{Se}_2$ ²⁷, respectively. With Pt doping into the Fe_2As_2 layers, the resistivity gradually decreases and metallic behavior emerges at high temperature. For samples with $0.015 < x < 0.023$, the resistivity still shows a semiconducting behavior but decreases below about 8 K without reaching zero, which can be regarded as a trace of superconductivity. With further Pt doping, zero resistivity was observed. The zero resistivity temperature $T_c(0)$ can reach the maximum of 13.6

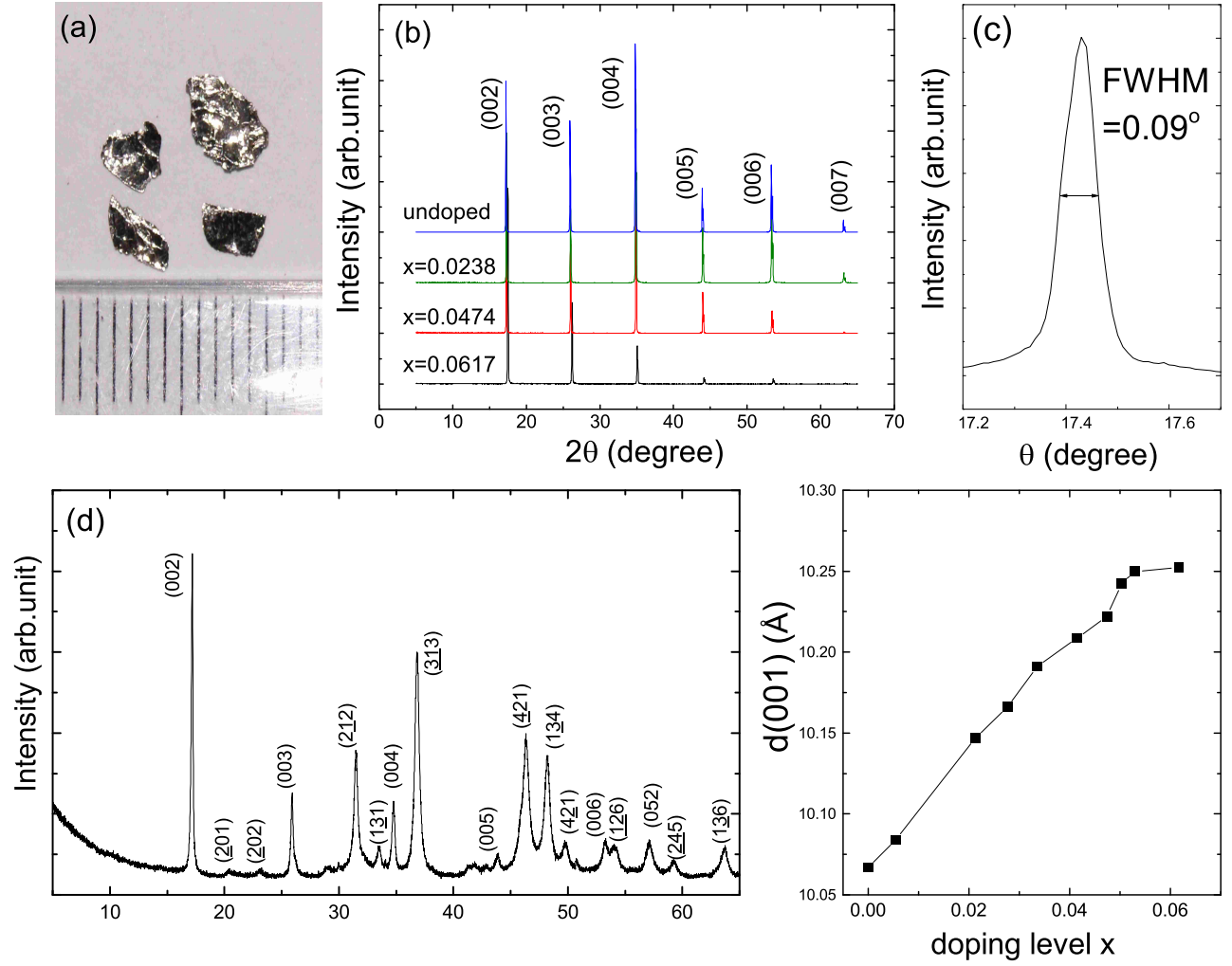


FIG. 1: (color online). (a) Photograph of single crystal pieces of $\text{Ca}_{10}(\text{Pt}_3\text{As}_8)((\text{Fe}_{1-x}\text{Pt}_x)_2\text{As}_2)_5$. (b) X-ray diffraction pattern of single crystals. (c) Rocking curve of the (004) reflection. (d) X-ray powder diffraction pattern of underdoped sample with doping level $x \approx 0.025$. (e) Doping dependence of the interlayer spacing of the Fe plane.

TABLE I: Atom ratios in the 10-3-8 phase

Sample number	Starting ratio Ca:Fe:Pt:As	EDS results Ca:Fe:Pt:As	doping level x
1	2 : 2 : 1.05 : 4	2 : 2.083 : 0.598 : 3.558	undoped
2	2 : 2 : 0.6 : 4	2 : 1.958 : 0.643 : 3.577	0.0213
3		2 : 1.960 : 0.675 : 3.527	0.0238
4		2 : 1.932 : 0.667 : 3.510	0.0335
5	2 : 2 : 0.7 : 4	2 : 1.946 : 0.682 : 3.540	0.0375
6		2 : 1.926 : 0.686 : 3.548	0.0415
7		2 : 1.957 : 0.707 : 3.560	0.0449
8	2 : 2 : 0.8 : 4	2 : 1.909 : 0.696 : 3.494	0.0474
9		2 : 1.942 : 0.716 : 3.499	0.0502
10	2 : 2 : 0.9 : 4	2 : 1.908 : 0.711 : 3.540	0.0530
11		2 : 1.888 : 0.727 : 3.550	0.0617
12	2 : 2 : 1.0 : 4	2 : 1.858 : 0.820 : 3.558	0.0981

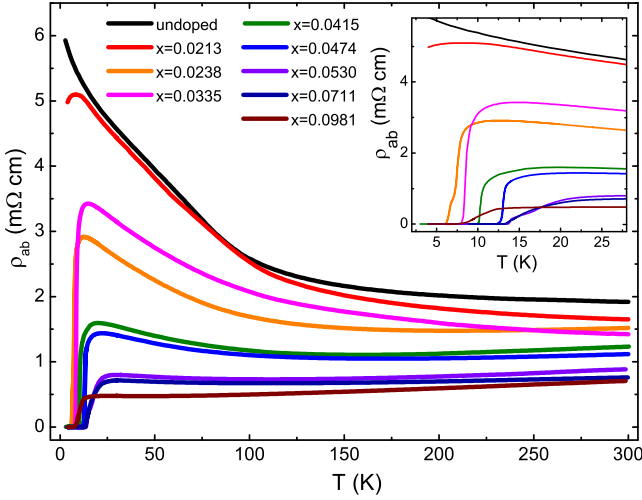


FIG. 2: (color online). The temperature dependence of resistivity for $\text{Ca}_{10}(\text{Pt}_3\text{As}_8)((\text{Fe}_{1-x}\text{Pt}_x)_2\text{As}_2)_5$ samples. The inset shows an expanded plot.

K in the samples with $x = 0.0530$ and $x = 0.0617$, and decreases with further doping when $x > 0.07$. Since the overdoped region was affected by the coexistence of 10-3-8 and 10-4-8 phase, we could not obtain the overdoped sample of pure 10-3-8 phase in which superconductivity is fully suppressed. In the whole superconducting region, most samples show a minimum in the normal-state resistivity curve. It should be mentioned that the temperature of resistivity minima, T_{\min} , has an overall trend of shift to lower temperature upon Pt doping. The typical temperature of resistivity minimum is about 150-200 K for the underdoped samples, 90-115 K for the optimally doped samples and 50-70 K for the overdoped samples. Neither abrupt slope break at T_{\min} nor other anomalies which can be attribute to a phase transition have ever been observed in the resistivity curves for all the samples, consistent with the previous reports^{18,20}. Below T_{\min} the resistivity curves show an upturn, which becomes less pronounced upon Pt doping. Similar phenomenon has been reported in 1111 Fe-based superconductors with element substitution within FeAs layers²⁸⁻³⁰ and superconducting phosphides such as BaRh_2P_2 ³¹. This behavior has been explained as an effect of weak localization or spin-flip scattering. However, the upturn is suppressed by Pt doping, which is contradict to the prediction of Anderson localization theory²⁹, meanwhile, it is hard to accept the Kondo-like scenario since Pt substitution does not introduce local moments as Co or Ni doping. Up to now the reason of this upturn remains unclear.

Figure 3 presents the temperature dependence of magnetic susceptibility χ of the superconducting samples measured under zero-field-cooling (ZFC) and field-cooling (FC) procedures by applying a magnetic field of 10 Oe along the ab -plane at low temperatures. All the samples with $x < 0.02$ show no diamagnetic signal above 2 K (not shown). For sample with $x = 0.0213$, in which zero

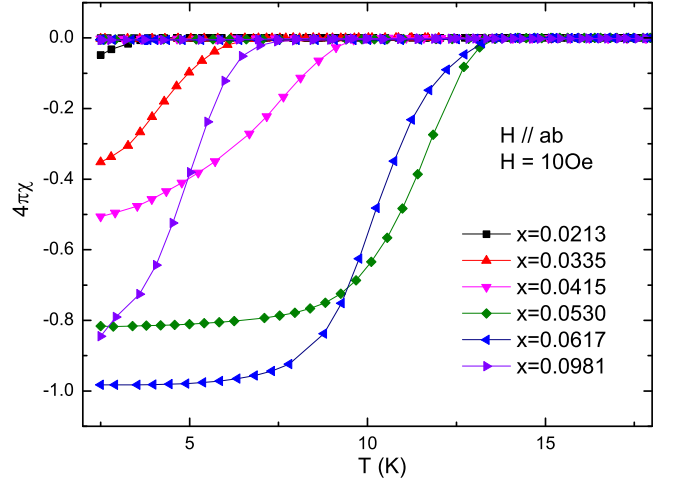


FIG. 3: (color online). The temperature dependence of in-plane magnetic susceptibility for superconducting $\text{Ca}_{10}(\text{Pt}_3\text{As}_8)((\text{Fe}_{1-x}\text{Pt}_x)_2\text{As}_2)_5$ samples with magnetic field 10 Oe.

resistivity was not observed, the diamagnetism signal can already be observed below the temperature $T_c = 4.3$ K, even though the magnetic shielding fraction is estimated to be less than 5%. Taking the non-uniform Pt distribution in sample into account, we suggest that the edge of superconducting region should be at a doping level between $x = 0.020$ and $x = 0.025$. The shielding fraction at 2.5 K exceeds 30% for samples with $x > 0.03$, reaches 80% for samples $x > 0.05$ and approximately 100% for the optimally doped sample with $x = 0.0617$, indicating bulk superconductivity in these samples. The superconducting transition temperature T_c in magnetic measurement is consistent with the zero resistivity temperature in the electric measurement. Samples with doping level of $x = 0.0530$ and $x = 0.0617$ have the maximum transition temperature in the 10-3-8 phase with $T_c = 13.6$ K, which is in consistent with the result reported by Kakiya et al.²⁰.

In Fig. 4(a), (b), (d) and (e), we present the resistivity data of two superconducting samples in low-temperature region under different fields. The samples studied were underdoped ones with $x = 0.0474$ and $T_c = 11.1$ K, and optimally doped sample with $x = 0.0617$ and $T_c = 13.6$ K (the value of T_c was determined by the susceptibility measurements). As there is a pronounced semiconductor-like behavior below T_{\min} and preceding the onset of the superconducting transition, a round maximum is formed at low temperature. The drop of resistivity below the temperature of this maximum is not very sharp. The interval between the maximum and the temperature at which resistivity reaches zero is as wide as about 15 K even in the optimally doped sample (see the inset of Fig. 2). As a result, it is rather difficult to determine the onset temperature of superconductivity from resistivity measurement. We chose three criteria of T_c as 90%, 50% and 10% of the normal state resistivity (determined as the local resistivity maxima at low temperature), and

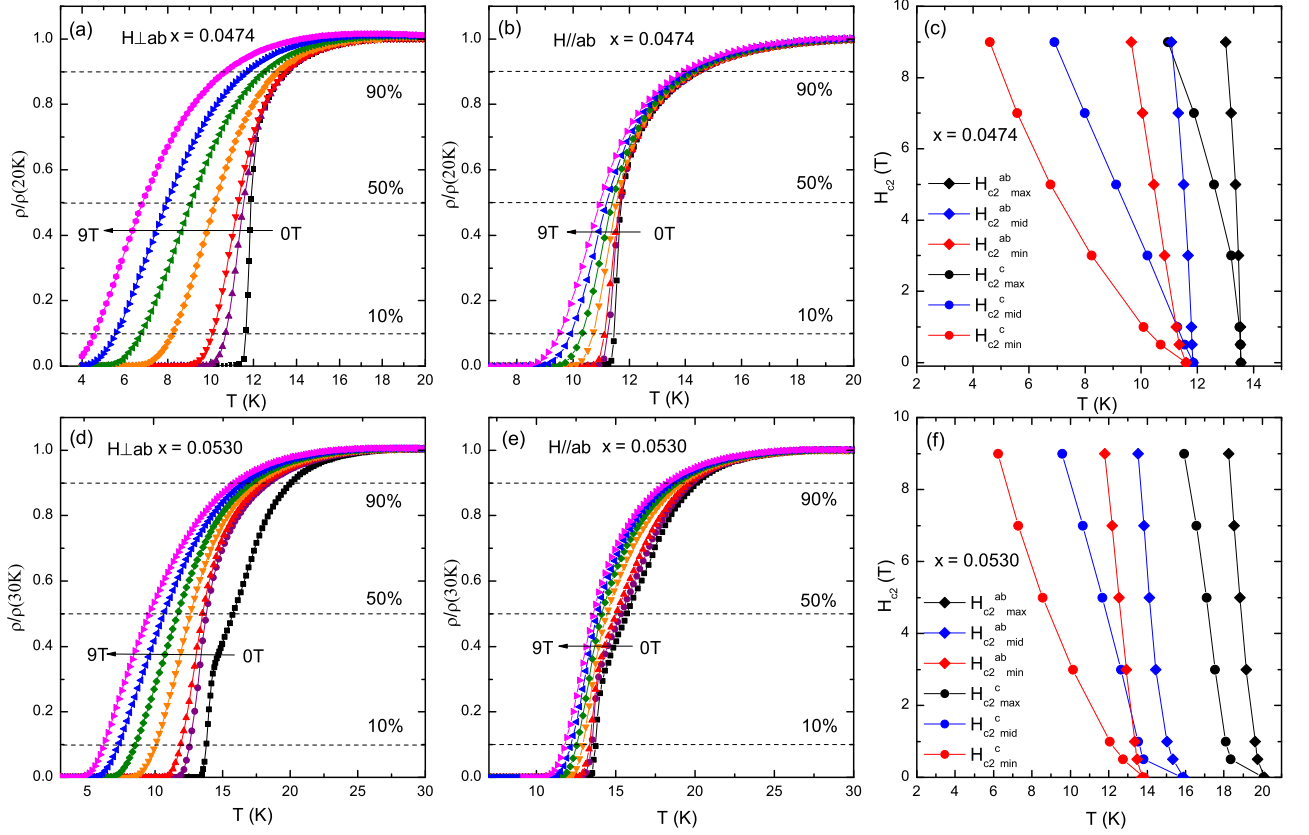


FIG. 4: (color online). In-plane electrical resistivity in magnetic fields ($H = 0$ T (black), 0.5 T (purple), 1 T (red), 3 T (orange), 5 T (olive), 7 T (blue) and 9 T (magenta), respectively) with (a)(d) $H \perp ab$ and (b)(e) $H // ab$ and upper critical fields under different criteria for $\text{Ca}_{10}(\text{Pt}_3\text{As}_8)((\text{Fe}_{1-x}\text{Pt}_x)_2\text{As}_2)_5$ samples with (a)(b)(c) $x = 0.0474$ and (d)(e)(f) $x = 0.0530$.

defined three critical field H_{C2}^{\max} , H_{C2}^{mid} and H_{C2}^{\min} following the three criteria respectively. All the critical fields are shown in Fig. 4(c) and (f). For the underdoped sample $x = 0.0474$, the behavior of critical fields are sensitive to the used criterion. When magnetic field applied perpendicular to ab plane, the H_{C2}^{\max} shows a negative curvature while H_{C2}^{\min} shows obviously positive curvature, and H_{C2}^{mid} has a nearly linear T -dependence. As for the case of $H // ab$, the results are similar but the curvatures are not so obvious. By using Werthamer-Helfand-Hohenberg formula³², the upper critical field at zero-temperature can be estimated from the initial slope $(dH_{C2}/dT)_{T=T_c}$. Under the 50% criterion, the value of $H_{C2}(0)$ is about 143.4 T for the configuration of $H // ab$ and about 14.13 T for $H \perp ab$. The anisotropy parameter $\Gamma = H_{C2}^{\parallel}/H_{C2}^{\perp}$ is derived to be about 10, which is much larger than those of $\text{NdFeAsO}_{0.89}\text{F}_{0.11}$ ($\Gamma \leq 6$)³⁷ and doped Ba-122 superconductors ($\Gamma \sim 1.5$ -2 for $\text{Ba}(\text{Fe}_{0.9}\text{Co}_{0.1})_2\text{As}_2$ ³⁴ and $\text{Ba}_{0.6}\text{K}_{0.4}\text{Fe}_2\text{As}_2$ ³⁵). Although the application of WHH model is questionable since this material was proved to be a multi-band system³⁶, the results at least indicated that the anisotropy of 10-3-8 phase is probably to be larger than those in 1111- and 122-type Fe-pnictides. The negative curvature of H_{C2}^{\max} is not common in the iron-based superconductors, and it may be affected seri-

ously by the magnetoresistance of normal state since it is difficult to fix the onset of superconductivity. On the other hand, H_{C2}^{\min} could be interpreted as the irreversibility field, and the upward behavior resembles those in $\text{LaFeAsO}_{0.89}\text{F}_{0.11}$ ³⁷ and $\text{Sr}_4\text{V}_2\text{O}_6\text{Fe}_2\text{As}_2$ ¹². For the optimally doped sample, an upward curvature was observed in all the critical field curves, and especially distinct for $H \perp ab$. Similar behavior has been reported in cuprates³⁸, MgB_2 ³⁹ and Fe-based 1111 superconductors^{33,40}. In 1111 Fe-pnictides this upward curvature was usually considered as a result of two-band effect^{37,40}. However, in the 10-3-8 phase the critical field curves show an upward bending near T_c , which is more pronounced than most of the other Fe-pnictide superconductors. This anomalous upturn has been theoretically interpreted as an effect of the two-dimensional nature and being associated with anisotropic Ginzburg-Landau behavior in the dirty limit⁴¹. Those properties of upper critical fields in the underdoped and optimally doped samples have been confirmed by the measurement on other several pieces of crystals with approximative doping concentration, and the shape of curves showed quite weak sample dependence. Additionally, the large interval exists between the resistivity curves under zero-field and $H = 0.5$ T in optimally doped samples might be due to the inhomogene-

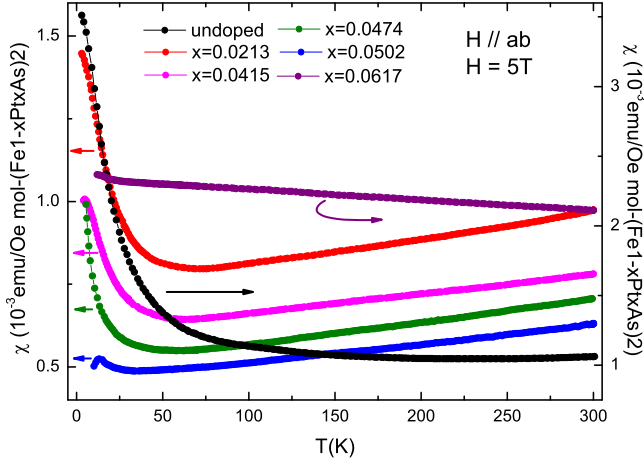


FIG. 5: (color online). The temperature dependence of in-plane magnetic susceptibility for $\text{Ca}_{10}(\text{Pt}_3\text{As}_8)((\text{Fe}_{1-x}\text{Pt}_x)_2\text{As}_2)_5$ single crystals under $H = 5$ T.

ity of Pt distribution, which formed small regions with higher T_c and in which the superconductivity is easily suppressed by low magnetic field. Nonetheless, the data of XRD and susceptibility afford no evidence that supports this assumption.

In order to confirm that there is no magnetic transition existing in the 10-3-8 phase, the normal-state susceptibility measurements were performed. Temperature dependence of the in-plane susceptibility (measured with magnetic field lying within the ab -plane) for samples with different Pt concentrations in the temperature range from 2 K to 300 K under $H = 5$ T are plotted in Fig. 5. For the undoped sample, the susceptibility χ first decreases when cooling from 300 K, and below about 270 K the slope diminishes gradually and then changes its sign smoothly at about 220-230 K. The temperature dependence of susceptibility is rather weak from 300 K to 100 K, and below ~ 75 K the susceptibility shows a Curie-like upturn. Again, no magnetic anomalies could be observed in the whole temperature region from 300 K to 2 K, which is different from iron-based parent compounds of 1111 and 122 systems. The paramagnetic behavior in the low-temperature region has been also reported in layered non-superconducting Fe-oxypnictides $\text{Sr}_3\text{Sc}_2\text{O}_5\text{Fe}_2\text{As}_2$ ⁴² and $\text{Sr}_4\text{Sc}_2\text{O}_6\text{Fe}_2\text{As}_2$ ²⁶. For the underdoped superconducting samples, the in-plane susceptibility exhibits a T -linear behavior above ~ 70 K, which is similar to those observed at high temperature in the underdoped $\text{LaO}_{1-x}\text{F}_x\text{FeAs}$ and 122-materials AeFe_2As_2 ($\text{Ae} = \text{Ca}, \text{Sr}, \text{Ba}$)^{5,23,43,44}. The slope of T -linear susceptibility decreases slightly upon Pt doping (with $6.63 \times 10^{-7} \text{ emu mol}^{-1} \text{ K}^{-1}$ for $x = 0.0213$, and $5.57 \times 10^{-7} \text{ emu mol}^{-1} \text{ K}^{-1}$ for $x = 0.0502$). The T -linear behavior has been explained as an effect of strong (π, π) SDW fluctuations, and the slope is determined by the square of the SDW amplitude with nesting momentum $\mathbf{Q} = (\pi, \pi)$ ⁴⁵. Since the slope of T -linear susceptibility in 10-3-8 phase lies between the value of the slope

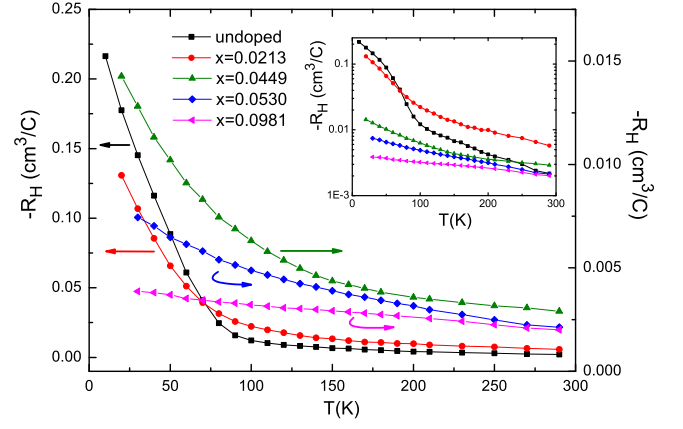


FIG. 6: (color online). The temperature dependence of Hall coefficient R_H for $\text{Ca}_{10}(\text{Pt}_3\text{As}_8)((\text{Fe}_{1-x}\text{Pt}_x)_2\text{As}_2)_5$ samples. The inset shows the same data on a logarithmic scale.

of Ni-doped LaFeAsO ²⁹ and Co-doped BaFe_2As_2 ⁵, we can conclude that even there is no SDW ordering in the 10-3-8 phase, strong AFM spin fluctuations still exist in this system and may play an important role in inducing superconductivity. At low temperature, the susceptibility of all the underdoped samples shows an obvious upturn, which has also been reported in many other Fe-pnictide superconductors^{28,29,46}. We attempted to fit the low temperature susceptibility of both undoped and underdoped samples using Curie-Weiss formula. For underdoped samples we obtained small effective moments ($\sim 0.1 \mu_B$ per Fe site) which shows considerable sample dependence, while for the undoped samples the Curie constant is one order of magnitude larger. Thus we believe that the Curie-Weiss-type behavior in the underdoped samples is likely to be extrinsic and could be ascribed to impurities and defects, as the case in 1111-materials, while in the semiconducting underdoped compound the paramagnetic behavior at low temperature might be intrinsic as in non-superconducting 32522 and 42622 systems. For the optimally doped and slightly overdoped samples, T -linear behavior is broken and χ is nearly temperature independent down to the onset of superconductivity. Both the behavior and the magnitude are similar to those in optimally doped 122 type Fe-pnictide superconductors^{21,47}.

Figure 6 shows the temperature-dependent Hall coefficients for $\text{Ca}_{10}(\text{Pt}_3\text{As}_8)((\text{Fe}_{1-x}\text{Pt}_x)_2\text{As}_2)_5$ crystals with different Pt content. We checked the linearity in H of the Hall voltage up to 5 T. For all of the samples the Hall coefficient R_H remains negative in whole temperature regime from T_c to 300 K, which indicates that electron-type charge carriers dominate the conduction in all the samples. The absolute value of R_H of the undoped sample is about twice as large as that of SmFeAsO ⁴⁸ at low temperature, but there is no anomaly in the slope of the R_H , which is related to magnetic transition. Nonetheless, the Hall coefficient of undoped sample as well as the underdoped samples shows a strong temperature de-

pendence at low temperatures, which suggests either a strong multiband effect or a spin related scattering effect⁴². With increasing Pt doping level, this temperature dependence becomes moderate and almost vanishes for the overdoped samples. The Hall concentration $n_H = 1/(eR_H)$, which represents carrier concentration in the single band model, however, does not follow a monotonic doping dependence at high temperature. As shown in the inset of Fig. 6, underdoped samples with $x = 0.0213$ and $x = 0.0449$ have larger R_H , that is, smaller Hall concentration than the undoped sample at room temperature. With enhancing Pt content, the Hall concentration first decreases in underdoped region and then turns to increase upon further doping. The turning point depends on temperature. All of these behaviors, except for the absence of SDW transition, are similar to those in $\text{Ba}(\text{Fe}_{1-x}\text{Co}_x)_2\text{As}_2$ ^{49,50}, which could be explained under a multi-band model as the competing effect of carrier doping and hole mobility decreasing in the underdoped region. Besides, the Hall concentration for the optimal doping at 200 K ($\sim 0.16e$ per Fe) is almost the same as that in the Co-doped Ba-122 system, but is about twice as large as that in the F doped SmFeAsO system.

Based on the data of transport and magnetic measurements shown above, an electronic phase diagram for $\text{Ca}_{10}(\text{Pt}_3\text{As}_8)((\text{Fe}_{1-x}\text{Pt}_x)_2\text{As}_2)_5$ system was summarized in Fig. 7. The undoped compound, $\text{Ca}_{10}(\text{Pt}_3\text{As}_8)(\text{Fe}_2\text{As}_2)_5$, is a heavily doped semiconductor without magnetic ordering, different to the parent compounds of 1111 and 122 Fe-pnictide superconductors, which are SDW-type bad metal. The Pt substitution on Fe site dopes electrons to the Fe_2As_2 layer, as is proved by the Hall coefficient measurements. About 2% Pt doping begins to introduce superconductivity, and T_c reaches its maximum $T_c^{\text{max}} = 13.6$ K in the doping range

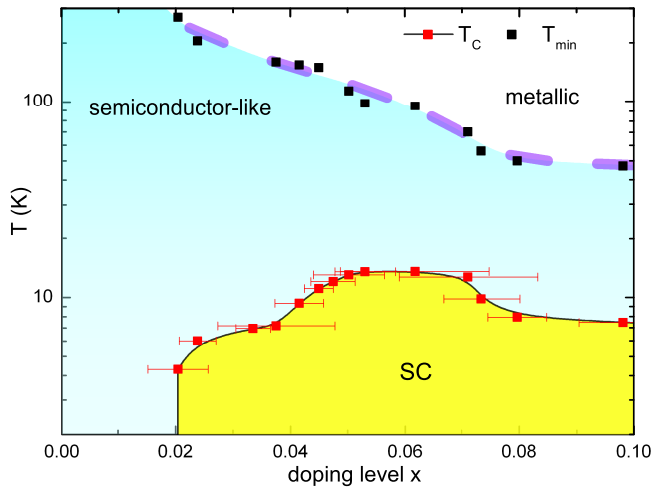


FIG. 7: (color online). Electronic phase diagram for $\text{Ca}_{10}(\text{Pt}_3\text{As}_8)((\text{Fe}_{1-x}\text{Pt}_x)_2\text{As}_2)_5$. T_{\min} indicates the resistivity minimum temperature. T_c was determined by susceptibility measurement.

$0.050 < x < 0.065$. Further Pt doping makes T_c decrease slowly. With the doping level up to $x \sim 0.1$ superconducting transition can still be observed at about 7.4 K and further doping leads the single 10-3-8 phase unable to be obtained. Therefore, the superconducting phase region is extremely asymmetric as in the Pt doped Ba-122 system⁵¹. The normal state is divided by the line of T_{\min} into semiconducting and metallic regions, which is similar to Co doped and Ni doped 1111 systems^{28,29}. The most extraordinary aspect of the phase diagram is the absence of SDW region which exists in the underdoped side of the electronic phase diagram for all the 11, 1111 and 122 Fe-pnictide materials^{7,52}. In the former phase diagram established by Cho et al.⁵³, the magnetic and superconducting phases are clearly separated. In this work we performed resistivity, susceptibility and Hall coefficient measurements, all of the data indicate the fact that there is actually neither SDW nor other type of magnetic order existing in the phase diagram of 10-3-8 system.

As mentioned above, static magnetic order is also absence in LiFeAs and "perov-FeAs" compounds. In the latter case, due to the large thickness of perovskite-type blocking layer, the distance between two nearest FePn layers is more than ~ 13 Å⁵⁵, which is much larger than other types of layered iron-pnictides. It is believed that the much stronger two-dimensional character compared to other Fe-pnictide superconductors, which causes relatively weak magnetic coupling between FeAs layers, is destructive to the antiferromagnetic correlation between the moments of Fe ions in the neighboring FeAs layers, and then prevents the system from forming a long range magnetic order^{26,42,55-57}. In the 10-3-8 phase, the distance between two neighboring FeAs layers is about 10.2 Å, which is smaller than that in perov-FeAs materials but still larger than in the 1111 materials ($d \sim 8.4$ - 8.9 Å) and 122 materials ($d \sim 5.8$ - 6.6 Å). The highly anisotropic 2D nature of $\text{Ca}_{10}(\text{Pt}_3\text{As}_8)((\text{Fe}_{1-x}\text{Pt}_x)_2\text{As}_2)_5$ is already indicated by our anisotropy parameter studies of upper critical field and the similar result by Ni et al¹⁸. Thus it is possible that the weak interlayer coupling suppresses the antiferromagnetic order in the 10-3-8 phase as in perov-FeAs materials. However, the linear T-dependence of susceptibility at high temperature indicates that antiferromagnetic spin fluctuation still exists in the 10-3-8 phase although magnetic ordering is suppressed. Strong antiferromagnetic spin fluctuation has been observed in LiFeAs ⁵⁴ and $(\text{Ca}_4\text{Al}_2\text{O}_{6-y})(\text{Fe}_2\text{As}_2)$ ⁵⁵, both of which have no magnetic order close to or coexisting with superconductivity. Therefore it is reasonable to conclude that there is also crucial relationship between AFM spin fluctuations and superconductivity in these materials, including the 10-3-8 phase, as in the other existing Fe-pnictide superconductors which have magnetic order in their parent compounds.

IV. CONCLUSION

In summary, high quality $\text{Ca}_{10}(\text{Pt}_3\text{As}_8)((\text{Fe}_{1-x}\text{Pt}_x)_2\text{As}_2)_5$ single crystals with doping level $0 \leq x < 0.1$ were successfully grown by self-flux method. A systematic study of the transport and magnetic properties of the single crystal samples was performed, and an electronic phase diagram was established. The undoped sample was a semiconductor without any type of magnetic order. Pt substitution on the Fe site dopes electrons into the Fe_2As_2 layers and introduces a metallic resistivity behavior and superconductivity. In the phase diagram there is no SDW region, which is a notable difference to the phase diagram of 1111 and 122 type Fe-pnictide materials. We argued that the absence of long-range AFM order is due to the strong 2D character of this system that revealed by the relatively large anisotropy parameter Γ . The extremely anisotropic nature weakens the interlayer coupling, as in the perovskite-type layered Fe-based compounds. Apart from that, the properties of superconducting samples were similar to other electron doped Fe-pnictide superconductors, indicating that the properties of this system is dominated by Fe_2As_2 layers. This is in consistent with previous results that the Pt_3As_8 layers couple only weakly with the Fe_2As_2

layers, and the contribution of density of states at the Fermi level from Pt is rather small^{19,36}. For underdoped samples, the magnetic susceptibility shows T-linear dependence in a wide temperature range, indicating strong magnetic fluctuation in this system. Thus it suggests that the mechanism of superconductivity of $\text{Ca}_{10}(\text{Pt}_3\text{As}_8)((\text{Fe}_{1-x}\text{Pt}_x)_2\text{As}_2)_5$ is similar to that in other iron-based superconductors. Being a special member of layered Fe-pnictide superconductor family with no magnetic order and shows variation of ground state from paramagnetic semiconductor to superconductor controlled by electron doping, the 10-3-8 phase is a good candidate to study the interplay between magnetic and superconductivity in Fe-pnictide superconductors. Further research on the magnetic fluctuation in this system may help to understanding the mechanism and nature of high-temperature superconductivity.

Acknowledgements

This work is supported by the National Natural Science Foundation of China (Grant No. 11190020 and No. 51021091), National Basic Research Program of China (973 Program, Grant No. 2012CB922002 and No. 2011CB00101) and Chinese Academy of Sciences.

-
- ¹ H. Chen, Y. Ren, Y. Qiu, Wei Bao, R. H. Liu, G. Wu, T. Wu, Y. L. Xie, X. F. Wang, Q. Huang and X. H. Chen, *Europhys. Lett.* **85**, 17006 (2009).
 - ² H. Luetkens, H.-H. Klauss, M. Kraken, F. J. Litterst, T. Dellmann, R. Klingeler, C. Hess, R. Khasanov, A. Amato, C. Baines, M. Kosmala, O. J. Schumann, M. Braden, J. Hamann-Borrero, N. Leps, A. Kondrat, G. Behr, J. Werner, and B. Büchner, *Nat. Mater.* **8**, 305 (2009).
 - ³ J. Zhao, Q. Huang, C. de la Cruz, S. L. Li, J. W. Lynn, Y. Chen, M. A. Green, G. F. Chen, G. Li, Z. Li, J. L. Luo, N. L. Wang and P. C. Dai, *Nat. Mater.* **7**, 953 (2008).
 - ⁴ A. J. Drew, Ch. Niedermayer, P. J. Baker, F. L. Pratt, S. J. Blundell, T. Lancaster, R. H. Liu, G. Wu, X. H. Chen, I. Watanabe, V. K. Malik, A. Dubroka, M. Rössle, K. W. Kim, C. Baines and C. Bernhard, *Nat. Mater.* **8**, 310 (2009).
 - ⁵ X. F. Wang, T. Wu, G. Wu, R. H. Liu, H. Chen, Y. L. Xie and X. H. Chen, *New Journal of Physics* **11**, 045003 (2009).
 - ⁶ Fa Wang and Dung-Hai Lee, *Science* **332**, 200 (2011).
 - ⁷ M. D. Lumsden and A. D. Christianson, *J. Phys.: Condens. Matter* **22**, 203203 (2010).
 - ⁸ I. I. Mazin, D. J. Singh, M. D. Johannes, and M. H. Du, *Phys. Rev. Lett.* **101**, 057003 (2008).
 - ⁹ A. V. Chubukov, D. V. Efremov, and I. Eremin, *Phys. Rev. B* **78**, 134512 (2008).
 - ¹⁰ V. Cvetkovic and Z. Tesanovic, *Europhys. Lett.* **85**, 37002 (2009).
 - ¹¹ S. V. Borisenko, V. B. Zabolotnyy, D. V. Evtushinsky, T. K. Kim, I. V. Morozov, A. N. Yaresko, A. A. Kordyuk, G. Behr, A. Vasiliev, R. Follath, and B. Büchner, *Phys. Rev. Lett.* **105**, 067002 (2010).
 - ¹² Xiyu Zhu, Fei Han, Gang Mu, Peng Cheng, Bing Shen, Bin Zeng, and Hai-Hu Wen, *Phys. Rev. B* **79**, 220512 (2009).
 - ¹³ Hiraku Ogino, Yasuaki Shimizu, Naoto Kawaguchi, Kohji Kishio, Jun-ichi Shimoyama, Tetsuya Tohei, and Yuichi Ikuhara, *Supercond. Sci. Technol.* **24**, 085020 (2011).
 - ¹⁴ Hiraku Ogino, Kenji Machida, Akiyasu Yamamoto, Kohji Kishio, Jun-ichi Shimoyama, Tetsuya Tohei, and Yuichi Ikuhara, *Supercond. Sci. Technol.* **23**, 115005 (2010).
 - ¹⁵ Parasharam M. Shirage, Kunihiro Kihou, Chul-Ho Lee, Hijiri Kito, Hiroshi Eisaki, and Akira Iyo, *J. Am. Chem. Soc.* **133**, 9630 (2011).
 - ¹⁶ Parasharam M. Shirage, Kunihiro Kihou, Chul-Ho Lee, Hijiri Kito, Hiroshi Eisaki, and Akira Iyo, *Appl. Phys. Lett.* **97**, 172506 (2010).
 - ¹⁷ H. Ogino, Y. Shimizu, K. Ushiyama, N. Kawaguchi, K. Kishio, J. Shimoyama, *J. Appl. Phys. Exp.* **3**, 63103 (2010).
 - ¹⁸ Ni Ni, Jared M. Allred, Benny C. Chan, and Robert Joseph Cava, *PNAS* **108**, 1019 (2011).
 - ¹⁹ C. Löhner, T. Stürzer, M. Tegel, R. Frankovsky, G. Friederichs, D. Johrendt, *Angewandte Chemie International Edition* **50**, 9195 (2011).
 - ²⁰ S. Kakiya, K. Kudo, Y. Nishikubo, K. Oku, E. Nishibori, H. Sawa, T. Yamamoto, T. Nozaka, and M. Nohara, *J. Phys. Soc. Jpn.* **80**, 093704 (2011).
 - ²¹ S. R. Saha, T. Drye, K. Kirshenbaum, N. P. Butch, P. Y. Zavalij, and J. Paglione, *J. Phys.: Condens. Matter* **22**, 072204 (2010).
 - ²² Kevin Kirshenbaum, Shanta R. Saha, Tyler Drye, and Johnpierre Paglione, *Phys. Rev. B* **82**, 144518 (2010).
 - ²³ X. F. Wang, T. Wu, G. Wu, H. Chen, Y. L. Xie, J. J. Ying,

- Y. J. Yan, R. H. Liu, and X. H. Chen, *Phys. Rev. Lett.* **102**, 117005 (2009).
- ²⁴ Michael A. McGuire, Andrew D. Christianson, Athena S. Sefat, Brian C. Sales, Mark D. Lumsden, Rongying Jin, E. Andrew Payzant, David Mandrus, Yanbing Luan, Veerle Keppens, Vijayalaksmi Varadarajan, Joseph W. Brill, Raphaël P. Hermann, Moulay T. Sougrati, Fernande Grandjean, Gary J. Long, *Phys. Rev. B* **78**, 094517 (2008).
 - ²⁵ Y. Kamihara, T. Watanabe, M. Hirano, and H. Hosono, *J. Am. Chem. Soc.* **130**, 3296(2008).
 - ²⁶ Y. L. Xie, R. H. Liu, T. Wu, G. Wu, Y. A. Song, D. Tan, X. F. Wang, H. Chen, J. J. Ying, Y. J. Yan, Q. J. Li and X. H. Chen, *Europhys. Lett.* **86**, 57007 (2009).
 - ²⁷ Y. J. Yan, M. Zhang, A. F. Wang, J. J. Ying, Z. Y. Li, W. Qin, X. G. Luo, J. Q. Li, Jiangping Hu, and X. H. Chen, *Sci. Rep.* **1**, 212 (2011).
 - ²⁸ C. Wang, Y. K. Li, Z. W. Zhu, S. Jiang, X. Lin, Y. K. Luo, S. Chi, L. J. Li, Z. Ren, M. He, H. Chen, Y. T. Wang, Q. Tao, G. H. Cao, and Z. A. Xu, *Phys. Rev. B* **79**, 054521 (2009).
 - ²⁹ Guanghan Cao, Shuai Jiang, Xiao Lin, Cao Wang, Yuke Li, Zhi Ren, Qian Tao, Chunmu Feng, Jianhui Dai, Zhuan Xu, and Fu-Chun Zhang *Phys. Rev. B* **79**, 174505 (2009).
 - ³⁰ S. J. Singh, J. Prakash, S. Patnaik, A. K. Ganguli, *Physica C* **470**, 1928 (2010).
 - ³¹ N. Berry, C. Capan, G. Seyfarth, A. D. Bianchi, J. Ziller, and Z. Fisk, *Phys. Rev. B* **79**, 180502 (2009).
 - ³² N. R. Werthamer, E. Helfand, and P. C. Hohenberg, *Phys. Rev.* **147**, 295 (1966).
 - ³³ Ying Jia, Peng Cheng, Lei Fang, Huiqian Luo, Huan Yang, Cong Ren, Lei Shan, Changzhi Gu and Hai-Hu Wen, *Appl. Phys. Lett.* **93**, 032503 (2008).
 - ³⁴ A. Yamamoto, J. Jaroszynski, C. Tarantini, L. Balicas, J. Jiang, A. Gurevich, D. C. Larbalestier, R. Jin, A. S. Sefat, M. A. McGuire, B. C. Sales, D. K. Christen, and D. Mandrus, *Appl. Phys. Lett.* **94**, 062511 (2009).
 - ³⁵ Zhao-Sheng Wang, Hui-Qian Luo, Cong Ren, and Hai-Hu Wen, *Phys. Rev. B* **78**, 140501 (2008).
 - ³⁶ M. Neupane, Chang Liu, S.-Y. Xu, Y. J. Wang, N. Ni, J. M. Allred, L. A. Wray, H. Lin, R. S. Markiewicz, A. Bansil, R. J. Cava, and M. Z. Hasan, *arXiv:1110.4687v1*.
 - ³⁷ F. Hunte, J. Jaroszynski, A. Gurevich, D. C. Larbalestier, R. Jin, A. S. Sefat, M. A. McGuire, B. C. Sales, D. K. Christen, and D. Mandrus, *Nature* **453**, 903 (2008).
 - ³⁸ M. S. Osofsky, R. J. Soulen, Jr., S. A. Wolf, J. M. Broto, H. Rakoto, J. C. Ousset, G. Coffe, S. Askenazy, P. Pari, I. Bozovic, J. N. Eckstein, and G. F. Virshup, *Phys. Rev. Lett.* **71**, 2315 (1993).
 - ³⁹ K.-H. Müller, G. Fuchs, A. Handstein, K. Nenkov, V. N. Narozhnyi, D. Eckert, *Journal of Alloys and Compounds* **322** (2001) L10.
 - ⁴⁰ J. Jaroszynski, F. Hunte, L. Balicas, Youn-jung Jo, I. Raicevic, A. Gurevich, D. C. Larbalestier, F. F. Balakirev, L. Fang, P. Cheng, Y. Jia, and H. H. Wen, *Phys. Rev. B* **78**, 174523 (2008).
 - ⁴¹ T. Schneider, *IBM Res.Dev.* **33**, 351 (1989).
 - ⁴² Xiyu Zhu, Fei Han, Gang Mu, Bin Zeng, Peng Cheng, Bing Shen, and Hai-Hu Wen, *Phys. Rev. B* **79**, 024516 (2009).
 - ⁴³ G. Wu, H. Chen, T. Wu, Y. L. Xie, Y. J. Yan, R. H. Liu, X. F. Wang, J. J. Ying and X. H. Chen, *J. Phys.: Condens. Matter* **20**, 422201 (2008).
 - ⁴⁴ R. Klingeler, N. Leps, I. Hellmann, A. Popa, U. Stockert, C. Hess, V. Kataev, H.-J. Grafe, F. Hammerath, G. Lang, S. Wurmehl, G. Behr, L. Harnagea, S. Singh, and B. Büchner, *Phys. Rev. B* **81**, 024506 (2010).
 - ⁴⁵ M. M. Korshunov, I. Eremin, D. V. Efremov, D. L. Maslov, and A. V. Chubukov, *Phys. Rev. Lett.* **102**, 236403 (2009).
 - ⁴⁶ R. E. Baumbach, J. J. Hamlin, L. Shu, D. A. Zocco, N. M. Crisosto, and M. B. Maple, *New Journal of Physics* **11**, 025018 (2009).
 - ⁴⁷ Neeraj Kumar, R. Nagalakshmi, R. Kulkarni, P. L. Paulose, A. K. Nigam, S. K. Dhar, and A. Thamizhave, *Phys. Rev. B* **79**, 012504 (2009).
 - ⁴⁸ R. H. Liu, G. Wu, T. Wu, D. F. Fang, H. Chen, S. Y. Li, K. Liu, Y. L. Xie, X. F. Wang, R. L. Yang, L. Ding, C. He, D. L. Feng, and X. H. Chen, *Phys. Rev. Lett.* **101**, 087001 (2008).
 - ⁴⁹ Lei Fang, Huiqian Luo, Peng Cheng, Zhaosheng Wang, Ying Jia, Gang Mu, Bing Shen, I. I. Mazin, Lei Shan, Cong Ren, and Hai-Hu Wen, *Phys. Rev. B* **80**, 140508 (2009).
 - ⁵⁰ F. Rullier-Albenque, D. Colson, A. Forget, and H. Alloul, *Phys. Rev. Lett.* **103**, 057001 (2009).
 - ⁵¹ Xiyu Zhu, Fei Han, Gang Mu, Peng Cheng, Jun Tang, Jing Ju, Katsumi Tanigaki, and Hai-Hu Wen, *Phys. Rev. B* **81**, 104525 (2010).
 - ⁵² P. C. Canfield, S. L. Budko, Ni Ni, J. Q. Yan, and A. Kracher, *Phys. Rev. B* **80**, 060501 (2009).
 - ⁵³ K. Cho, M. A. Tanatar, H. Kim, W. E. Straszheim, N. Ni, R. J. Cava, and R. Prozorov, *arXiv:1111.1003v1*
 - ⁵⁴ A. E. Taylor, M. J. Pitcher, R. A. Ewings, T. G. Perring, S. J. Clarke, and A. T. Boothroyd, *Phys. Rev. B* **83**, 220514 (2011).
 - ⁵⁵ H. Kinouchi, H. Mukuda, M. Yashima, Y. Kitaoka, P.M. Shirage, H. Eisaki, and A. Iyo, *Phys. Rev. Lett.* **107**, 047002 (2011).
 - ⁵⁶ Athena S. Sefat, David J. Singh, V. Ovidiu Garlea, Yuri L. Zuev, Michael A. McGuire, Brian C. Sales, *Physica C* **471**, 143 (2011).
 - ⁵⁷ J. Munevar, D. R. Sánchez, M. Alzamora, E. Baggio-Saitovitch, J. P. Carlo, T. Goko, A. A. Acze, T. J. Williams, G. M. Luke, Hai-Hu Wen, Xiyu Zhu, Fei Han, and Y. J. Uemura, *Phys. Rev. B* **84**, 024527 (2011).